



Pharmaceutics, Drug Delivery and Pharmaceutical Technology

Micelle Formation and Phase Separation of Poloxamer 188 and Preservative Molecules in Aqueous Solutions Studied by Small Angle X-ray Scattering



Rachel R. Ford^{a,b,*}, Peter H. Gilbert^{a,b}, Richard Gillilan^c, Qingqiu Huang^c,
Róisín Donnelly^a, Ken K. Qian^d, David P. Allen^d, Norman J. Wagner^a, Yun Liu^{a,b}

^a Department of Chemical & Biomolecular Engineering, Center for Neutron Science, University of Delaware, Newark, DE, 19716, United States

^b NIST Center for Neutron Research, National Institute of Standards and Technology, Gaithersburg, MD, 20899, United States

^c Center for High-Energy X-ray Sciences at CHESS, Cornell University, Ithaca, NY, 14853, United States

^d Eli Lilly and Company, Indianapolis, IN, 46225, United States

ARTICLE INFO

Article history:

Received 22 April 2022

Revised 16 September 2022

Accepted 16 September 2022

Available online 21 September 2022

Keywords:

Excipient(s)

Formulation

Micelle(s)

Phase diagram(s)

Surfactant(s)

ABSTRACT

Multi-injection pharmaceutical products such as insulin must be formulated to prevent aggregation and microbial contamination. Small-molecule preservatives and nonionic surfactants such as poloxamer 188 (P188) are thus often employed in protein drug formulations. However, mixtures of preservatives and surfactants can induce aggregation and even phase separation over time, despite the fact that all components are well dissolvable when used alone in aqueous solution. A systematic study is conducted here to understand the phase behavior and morphological causes of aggregation of P188 in the presence of the preservatives phenol and benzyl alcohol, primarily using small-angle x-ray scattering (SAXS). Based on SAXS results, P188 remains as unimers in solution when below a certain phenol concentration. Upon increasing the phenol concentration, a regime of micelle formation is observed due to the interaction between P188 and phenol. Further increasing the phenol concentration causes mixtures to become turbid and phase-separate over time. The effect of benzyl alcohol on the phase behavior is also investigated.

© 2022 American Pharmacists Association. Published by Elsevier Inc. All rights reserved.

Introduction

Solutions of injectable biopharmaceutical products must meet particle size and turbidity requirements to ensure their safety and to preserve drug activity.^{1–3} As aggregation can lead to denaturation or cause immunological responses,^{4,5} protein solutions need to be formulated to prevent the growth of large aggregates. Thus, drug formulations often require stabilizing excipients such as nonionic surfactants. Commonly used nonionic surfactants employed in protein drug formulations include polysorbate 20 (PS20), polysorbate 80 (PS80), and poloxamer 188 (P188).⁶ Also known by the trade names Kolliphor P 188, Lutrol F68, Pluronic F68, and Synperonic F68, P188 is a thermoresponsive ABA triblock copolymer of polyethylene oxide and polypropylene oxide, wherein the internal hydrophobic propylene oxide block constitutes a mass fraction of approximately 20 %.

Abbreviations: BzOH, benzyl alcohol; CMC, critical micelle concentration; CMT, critical micelle temperature; P188, poloxamer 188; PhOH, phenol; PS20, polysorbate 20; PS80, polysorbate 80; SANS, small-angle neutron scattering; SAXS, small-angle x-ray scattering.

* Corresponding author.

E-mail address: rachel.ford@nist.gov (R.R. Ford).

P188 has been increasingly utilized in pharmaceutical applications due to precise control over chain length and stability to hydrolysis conditions, in contrast to traditional polysorbate surfactants.^{2,3,6–13} Additionally, P188 has been used along with small molecule preservatives in several biologic drug products, such as Gonal-f,¹⁴ Norditropepin,¹⁵ and Omnitrope.¹⁶

However, it has been reported that the combination of P188 with small molecule preservatives or with other surfactants can induce aggregate formation.^{10,17} Jacobs et al. investigated the interactions of phenol with P188, and reported turbidity in compositions where the P188:phenol ratio was sufficiently low, despite being well below the phenol solubility limit.¹⁷ Similar turbidity was reported in PS80/preservative mixtures by Gilbert et al.¹⁸; small-angle neutron scattering (SANS) experiments revealed pronounced time-dependent aggregation of PS80 micelles upon the addition of the preservative *m*-cresol, also at concentrations of PS80 and *m*-cresol that are well below their individual solubility limits. Structural changes were observed for several days after mixing the two excipients. Their results indicated two stages of structure development: initial "fast" changes in morphology occur as aggregation begins, and a slower process of coalescence into larger aggregates ensues.¹⁹ While aggregation itself does not

necessarily present a safety concern for drug products, understanding the aggregation mechanisms in both the PS80/*m*-cresol system and the P188/phenol system is useful for industrial utilization of these systems, and warrants further investigation.

Here, we have systematically explored the molecular and morphological causes for aggregation in P188/preservative solutions, primarily using small-angle X-ray scattering (SAXS). We have sought to investigate complex formation due to the interplay of P188 and preservative molecules, and their solution structures that lead to turbidity in P188/preservative formulations. It is also noted that in contrast to the PS80/*m*-cresol system, where PS80 already exists as micelles prior to the addition of *m*-cresol, P188 molecules have been observed to be unimers at room temperature.²⁰ Thus, the molecular driving force for apparent aggregation in P188/preservative solutions could be different, and has remained unknown until now.

Materials and experimental section

Materials

Ploxamer 188 (BASF; Kolliphor P 188; 8780 g/mol; Bio Grade; Lot #GNA21721B), phenol (Sigma-Aldrich, 94.1 g/mol; Lot #BCBW2964), and anhydrous benzyl alcohol (Sigma-Aldrich, 108.1 g/mol; Batch #0000213391) were purchased by Eli Lilly & Company and were used as received. Monobasic sodium phosphate monohydrate (Sigma-Aldrich, 138.0 g/mol) and dibasic sodium phosphate heptahydrate (Sigma-Aldrich, 268.1 g/mol) were purchased from Sigma Aldrich and used as received. Samples were prepared using Milli-Q water. Caution: phenol and benzyl alcohol are hazardous compounds. Only handle them inside a fume hood while wearing gloves and safety glasses, as described in their respective safety data sheets.

Sample preparation and visual assessment

All samples were prepared from stock solutions in 5 mmol/L phosphate buffer. The preparation of a set of stock solutions and a 1 mL sample are described as a representation of all sample preparation. Phosphate buffer was made by combining 40.35 mg (0.1505 mmol) of dibasic sodium phosphate heptahydrate, 49.61 mg (0.3595 mmol) of monobasic sodium phosphate monohydrate, and 99.91 mL of H₂O in a plastic bottle. The bottle was placed on its side on an orbital shaker operating at 150 rpm (2.5 Hz) for 1 h to 2 h to mix; the resultant buffer contained 5 mmol/L sodium phosphate with an approximate pH of 6.7. A stock solution of P188 in phosphate buffer at 40 mg/mL was prepared by combining 0.8 g P188 with 19.2 mL buffer in a plastic bottle. The bottle was placed on its side on an orbital shaker operating at 150 rpm (2.5 Hz) for 1 h to 2 h to mix then set on the benchtop for at least 10 min prior to use, to allow bubbles to dissipate. A stock solution of phenol in phosphate buffer at 40 mg/mL was prepared by combining 0.8 g phenol with 19.2 mL buffer in a plastic bottle; the bottle was placed on its side on an orbital shaker operating at 150 rpm (2.5 Hz) for 1 h to 2 h to mix. A stock solution of benzyl alcohol in phosphate buffer at 18 mg/mL was prepared by combining 0.36 g (346 μL) benzyl alcohol with 19.654 mL buffer in a plastic bottle; the bottle was placed on its side on an orbital shaker operating at 150 rpm (2.5 Hz) for 1 h to 2 h to mix. A 1 mL sample containing 2.5 mg/mL P188, 5 mg/mL phenol, and 9 mg/mL benzyl alcohol was prepared from these stocks by combining 0.0625 mL P188 stock solution, 0.3125 mL buffer, 0.5 mL benzyl alcohol stock solution, and 0.125 mL phenol stock solution, in that order in a glass vial. The vial was inverted over and over for about 10 s to mix the components. Often, due to a high local concentration of phenol when its stock was initially added, wisps of cloudy material developed in the vial, which dissipated upon mixing. In all cases, phenol was added last to the sample. To determine the turbidity boundary in phase

diagrams at 22°C, samples were evaluated 1 h after the addition of phenol.

Small-angle X-ray scattering measurements

Small-angle X-ray scattering (SAXS) measurements were performed at the ID-7A1 High Pressure Bio-SAXS beamline at the Cornell High Energy Synchrotron Source. Measurements were conducted at ambient pressure and 20°C. This instrument employs a photon energy of ≈ 9.8 keV with 1.5% bandwidth, has a sample-to-detector distance of 1648 mm, and probes scattering wavevector, *Q*, values of 0.009 Å⁻¹ to 0.52 Å⁻¹. The detector was calibrated to the beam center using silver behenate and the instrument was calibrated for absolute intensity using the known value of 0.016 cm⁻¹ for water. The sample chamber was a capillary that oscillated the 60 μL sample back and forth through the beam to minimize the damage from radiation. Each measurement was made by exposing the oscillating sample to the beam five times for 1 s or 2 s per exposure; these exposures were then averaged together to improve counting statistics.

Data reduction was performed using BioXTAS RAW software.²¹ Raw data from the instrument was loaded into RAW as .h5 files, which were already converted to I vs. *Q*. Five replicate exposures were averaged together and the similarly averaged buffer background was subtracted to obtain reduced data as .dat files. After converting to .txt files, reduced data were then binned to 40 points per decade in *Q*, with intensities being averaged within each bin and set to the central *Q*-value of the bin. Binning was done using a python script, which is available in the Supplementary Information section online.

SAXS data analysis

In SAXS experiments, intensity is measured as a function of scattering wavevector, *Q*, which is related to the wavelength, λ, of incident x-rays and the angle, θ, between the incident and the scattered wavevectors as

$$Q = \frac{4\pi \sin \frac{\theta}{2}}{\lambda} \quad (1)$$

SAXS intensity for a solution sample can be generally expressed as

$$I(Q) = \Delta \rho^2 \varphi V_p S(Q) P(Q) + I_{bgd} \quad (2)$$

where Δρ² is the square of the difference in scattering length density, ρ, between the scattering particle and the solvent, φ is the volume fraction of the scattering particle, V_p is the volume of a single scattering particle, S(*Q*) is the inter-particle structure factor, which describes inter-particle correlation, P(*Q*) is the normalized form factor, which describes the structure of the individual scattering particles, and I_{bgd} is the scattering background.

For dilute solutions, S(*Q*) ≈ 1 and at sufficiently low *Q* the Guinier approximation holds that the normalized form factor is given by

$$P(Q) = e^{-\frac{1}{3}Q^2 R_g^2} \quad (3)$$

where R_g is the radius of gyration. Therefore, the background-subtracted intensity is

$$I(Q) - I_{bgd} = \Delta \rho^2 \varphi V_p e^{-\frac{1}{3}Q^2 R_g^2} \quad (4)$$

At *Q* = 0, the intensity is Δρ²φV_p, which can be represented as the single parameter I₀. Taking the natural log of both sides gives

$$\ln(I(Q) - I_{bgd}) = \ln I_0 - \frac{R_g^2}{3} Q^2 \quad (5)$$

In a plot of ln(I(*Q*) - I_{bgd}) vs. *Q*², data is linear at low-*Q* where the y-intercept is the natural log of I₀ and the slope is related to the

square of R_g . Fitting the data at low- Q (Guinier analysis) to obtain I_0 and R_g was performed in Igor Pro 8.04 using the NCNR Analysis Macros.²² The Guinier approximation holds regardless of the morphology of scattering particles.

In addition to Guinier analysis, some samples were also fit to the polydisperse Gaussian coil model²³ using SasView²⁴ (<https://www.sasview.org/>). This model holds for a polymer in a theta solvent (i.e., the polymer has no preference between self-association and dissolution in the solvent), such that the set of monomer-monomer distances for all pairs of monomers in the chain follows a Gaussian distribution. The form factor for the polydisperse Gaussian coil²³ is given by

$$P_{\text{Gauss}}(Q) = \frac{2\left((1+UZ)^{-1/U} + Z - 1\right)}{(1+U)Z^2} \quad (6)$$

where

$$Z = \frac{(QR_g)^2}{1+2U} \quad (7)$$

and U is related to the polydispersity ratio as

$$U = \frac{M_w}{M_n} - 1 \quad (8)$$

Polydispersity in molecular weight is described by a Schulz-Zimm-like distribution. The overall scattering intensity is modeled as

$$I(Q) = \text{scale} \cdot I_0 \cdot P_{\text{Gauss}}(Q) + bgd \quad (9)$$

where I_0 is $\Delta\rho^2\phi V_p$ for the polymer. For fitting to a Gaussian coil, I_0 was held fixed at the value determined by Guinier analysis. All other parameters were allowed to vary.

Results

The turbidity of the P188/phenol samples were investigated by visual evaluation, with an exemplary picture of the samples shown in Fig. 1 and Fig. S6 of the Supplementary Information. A previous study indicated that for the PS80/*m*-cresol system, there are slow kinetics for some samples, which appear to be transparent initially and become turbid after a day or two.^{18,19} However, we observed that all samples that were transparent at the time of preparation remained transparent for as long as we monitored them, which is approximately six weeks. Within our studied concentration range, all samples that were turbid at the time of preparation remained turbid after a day. Samples that turned turbid tended to phase separate on a longer time scale over the course of a few days, forming a white powder precipitate or a film deposited on the walls of the vessel and leaving a relatively clear supernatant. To be consistent, the turbidity of all samples were assessed and reported 1 h after preparation. For a

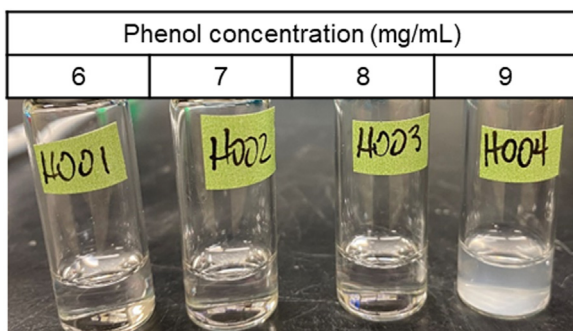


Fig. 1. The addition of phenol to an aqueous solution of P188 causes the mixture to become turbid at certain compositions. All vials contain 0.4 mg/mL P188 in 5 mmol/L phosphate buffer.

representative series of compositions, we validated our visual assessment of turbidity with ultraviolet-visible light spectrophotometry (Fig. S5, Supplementary Information). A sharp decrease in transmittance occurred at the visually determined onset of turbidity. The relative refractive indices are 1.54,²⁵ 1.465,²⁶ and 1.33²⁶ for phenol, P188, and water respectively. When P188 and phenol form aggregates with very large sizes (such as micrometer-sized aggregates), the refractive index of the aggregates is thus larger than the solvent with a refractive index of 1.33. This refractive index difference causes the scattering of light at all wavelengths. When the sample reaches the turbid region, there are many large aggregates that scatter light, causing the sample to become white. As benzyl alcohol is also used in some formulations, we examined the effect of benzyl alcohol on the turbidity boundary as a function of phenol concentration. Adding benzyl alcohol does not introduce any kinetic effects in transparent samples by visual evaluation.

Phase diagrams

As turbidity was observed in mixtures of P188 and phenol well below the phenol aqueous solubility limit of 80 mg/mL, we sought to map out the turbidity boundaries for a variety of P188 and phenol concentrations, and for two concentrations of benzyl alcohol, 0 mg/mL and 9 mg/mL (Fig. 2). The concentration of benzyl alcohol was selected based on the dosage used in formulations. The concentrations evaluated are relevant to pharmaceutical formulations.

The boundary between transparent and turbid was determined visually after allowing solutions to mix without agitation for at least 1 h (Fig. 2). In all cases tested, samples that were transparent upon initial mixing remained transparent for several weeks when held at room temperature or under refrigeration. The longest we visually monitored transparent samples was approximately six weeks. The turbidity boundary exhibits modest dependence on P188 concentration (C_{P188}), but is primarily dictated by phenol content—wherein the threshold for turbidity is nearly an order of magnitude below the solubility limit for phenol in aqueous buffer, which is approximately 80 mg/mL. Interestingly, as C_{P188} is decreased, the phenol turbidity threshold decreases also. Given that phenol is soluble for $C_{\text{P188}} = 0$ at the concentrations examined, this means the turbidity boundary forms an asymmetric U-shaped curve.

The incorporation of 9 mg/mL benzyl alcohol leads to a decrease in the turbidity boundary of approximately 2 mg/mL phenol for a given concentration of P188. Although benzyl alcohol is more hydrophobic than phenol, mixtures of benzyl alcohol and P188 without phenol do not become turbid up to 18 mg/mL benzyl alcohol. This result is counter to what one would predict based on the hydrophilic-lipophilic balance framework typically employed in the design of formulations.

In addition to visual evaluation, we also characterized the solution morphology of P188 and aggregates for transparent samples using small-angle X-ray scattering (SAXS), and found that two phase regimes exist within transparent samples. For lower concentrations of phenol, all components remained dispersed as unimers in solution (unimer regime; below the green lines in Fig. 2). Higher concentrations of phenol led to micelle formation with P188 (micelle regime; between the green and red lines in Fig. 2). The specific phenol concentration where this transition occurs is dependent on the concentration of benzyl alcohol, and is between 4 mg/mL and 6 mg/mL phenol. This is discussed in detail later in the paper.

Solution behavior of P188

To understand the morphology of P188 in solution alone, we first measured SAXS patterns of P188-only solutions in 5 mmol/L phosphate buffer at room temperature (20°C) (Fig. 3). According to

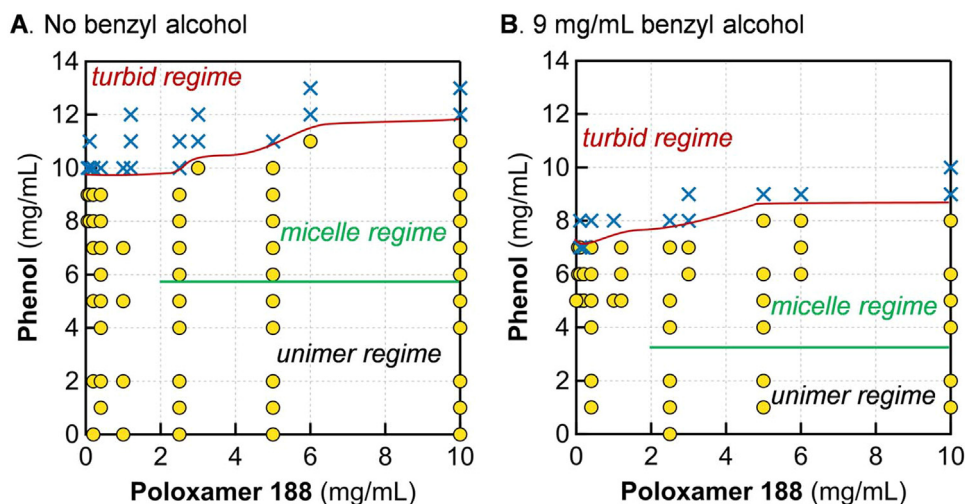


Fig. 2. Instability in P188/preservative mixtures. Boundaries for the micelle regime were determined by SAXS measurements. The boundary for micelle formation is unknown for $c_{P188} < 2.5$ mg/mL due to contrast/instrument limitations of SAXS. The presence of 9 mg/mL benzyl alcohol (B) causes the boundaries of both turbidity and micelle formation to shift down by ≈ 2 mg/mL phenol, compared to the P188/phenol system (A). Solutions were in 5 mmol/L phosphate buffer at room temperature (20°C to 22°C). Yellow circles denote transparent samples and blue Xs denote turbid samples, visually determined after 1 h of mixing. Phenol alone is soluble in aqueous buffer up to 80 mg/mL. Benzyl alcohol is soluble up to 40 mg/mL.

Guinier fits of SAXS data, the R_g of P188 was ≈ 30 Å and did not appreciably vary across all concentrations of P188 explored, apart from a modest decrease for $c_{P188} = 10$ mg/mL (Fig. 3B). The hydrodynamic radius of P188 at 10 mg/mL was found to be 32 Å by dynamic light scattering (see Fig. S3 in Supplementary Information), which is consistent with previous studies.²⁰ The apparent decrease in R_g for $c_{P188} = 10$ mg/mL is due to inter-molecular interactions between P188 molecules at high concentration. Scaling I_0 to P188 concentration provides a quantitative means of assessing the molecular weight of the scattering species as a function of the concentration of P188. Similarly to the trend for R_g , I_0/c_{P188} does not substantially change with increasing P188 concentration, meaning the aggregation number and molecular mass are unchanged. The consistency in R_g and I_0/c_{P188} with P188 concentration indicates that P188 remains as unimers at all concentrations probed in this study, up to 10 mg/mL P188, when there are no other excipient molecules. The scattering data were also fit with the polydisperse Gaussian coil model, showing that

individual P188 chains exist as random coils (Fig. 3A). The list of R_g and I_0 from Guinier analysis of all samples is given in Table S1 of the Supplementary Information. The fit parameters for the polydisperse Gaussian model are listed in Table S2 of the Supplementary Information.

Micelle formation induced by phenol

Having explored solution structure of P188 alone, we examined the effect of phenol on P188 structure and complex formation due to the interaction between P188 and phenol. As shown in Fig. 4A, for a fixed P188 concentration at 2.5 mg/mL, adding phenol to the P188 solution does not alter the SAXS scattering pattern up to 5 mg/mL of phenol. Thus, P188 remains as unimers in buffer even with added phenol molecules. However, upon further increasing the phenol concentration, the SAXS patterns show a significant change at $Q < 0.1$ Å⁻¹ indicating that the size and molecular mass of the

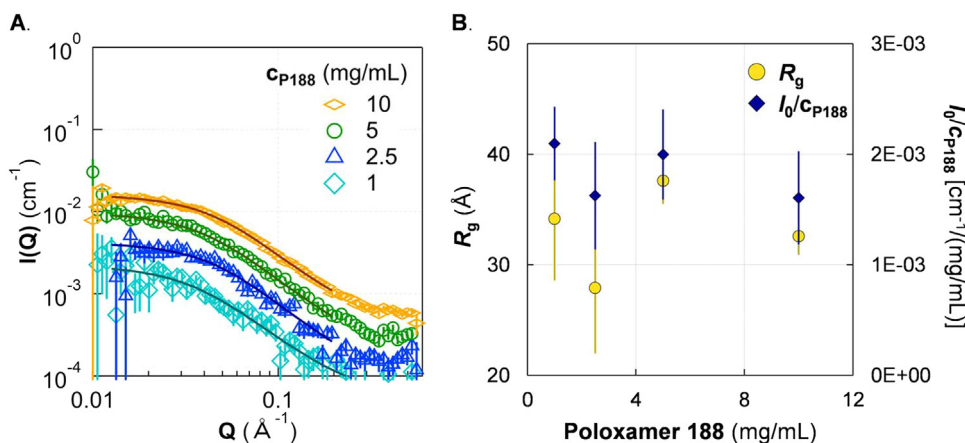


Fig. 3. SAXS of P188 shows no evidence of micellization up to 10 mg/mL. A. SAXS of P188 solutions (markers) with fits (lines) to a polydisperse Gaussian coil polymer model. B. Guinier analysis showed that both the radius of gyration (R_g ; left axis) and the concentration-scaled $I(Q=0)$ (I_0/c_{P188} ; right axis) are generally constant with increasing c_{P188} . It is possible that I_0/c_{P188} decreases slightly, which can be attributed to excluded volume effects. The lack of growth in either R_g or I_0/c_{P188} indicates that P188 does not form micelles at ≤ 10 mg/mL at 20°C . Solutions were in 5 mmol/L phosphate buffer. Error bars are shown for all data and represent one standard deviation. Some error bars are covered by the markers.

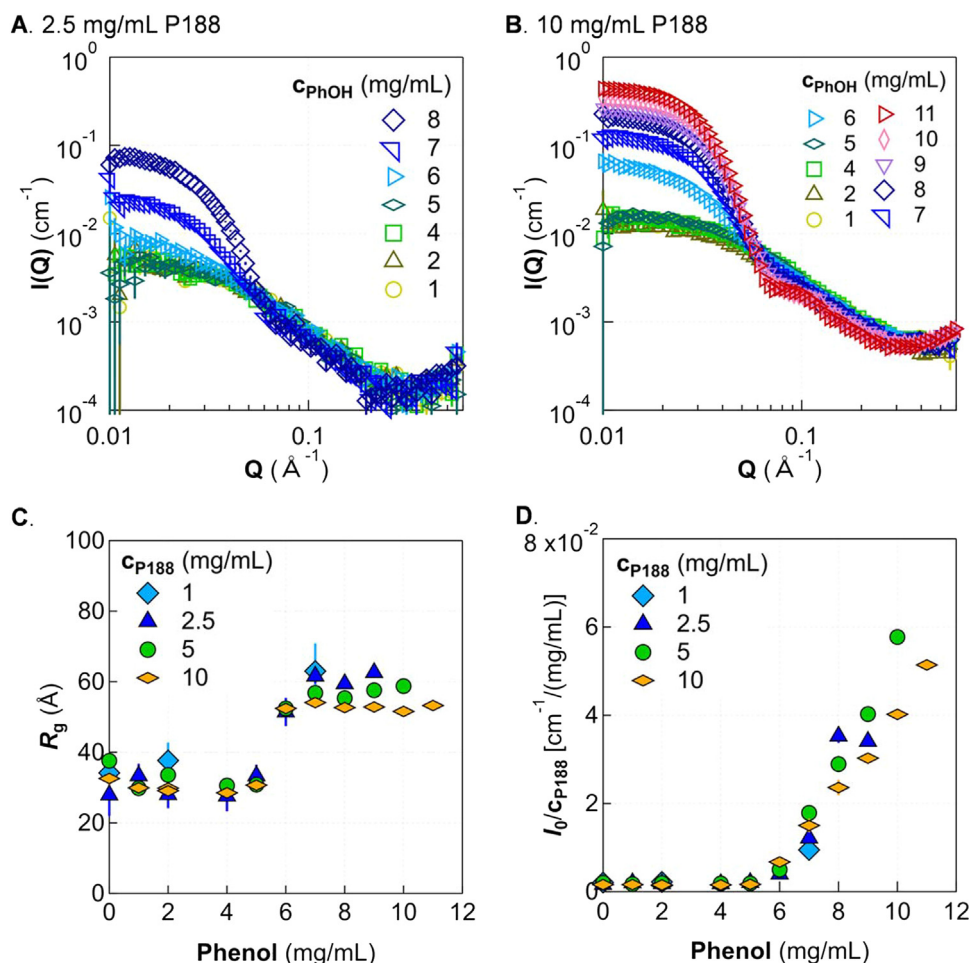


Fig. 4. Morphology change with increasing phenol and P188 concentration. SAXS patterns are shown for two representative concentrations of P188, 2.5 mg/mL (A) and 10 mg/mL (B). Guinier analysis shows that R_g increases after a certain phenol concentration then tapers off as phenol is increased further (C), while I_0/c_{P188} continually increases (D). Solutions were in 5 mmol/L phosphate buffer at 20°C. Error bars are shown for all data and represent one standard deviation. Some error bars are covered by the markers.

individual particles in solutions becomes larger. We also studied phenol in buffer using SAXS. At all the concentrations investigated here, the SAXS pattern of phenol in buffer is indistinguishable from that of pure buffer (Fig. S1, Supplementary Information). Thus, phenol by itself does not form any large aggregates in the investigated concentration region; the change in the SAXS pattern of P188 with phenol is due to interactions between phenol and P188.

We were surprised by this observed aggregation of P188 and phenol at higher concentrations of the latter ($c_{PhOH} > 6$ mg/mL). The solubility of phenol in water is 80 mg/ml at 25°C and the solubility of P188 in water is hundreds of milligrams per milliliter, where solubility can vary by batch²⁷—both solubility limits are much higher than the concentrations investigated here. Whereas P188 and phenol exist as unassociated molecules when dissolved alone in water, they interact to form micelles. Adding soluble co-solvent molecules to a micelle system is known to shift the transition concentration of micelle formation. Phenol has been observed to associate with cationic²⁸ and nonionic^{29,30} micelles to decrease the critical micelle temperature (CMT) of the respective system. For the concentrations studied here, the CMT of P188 alone is above 30°C,²⁰ while the addition of phenol shifts the CMT to below room temperature. Guinier analysis provides insight into the structural origin of micelle formation, which we discuss later in this paper.

The transition from the unimer region to the micelle region of P188/phenol solutions is also studied at other concentrations of P188. Fig. 4B shows the SAXS pattern for a solution of 10 mg/mL

P188 with 1 mg/mL to 8 mg/mL phenol. The results are similar to those in Fig. 4A. The micelle transition occurs at approximately 6 mg/mL phenol. Fig. 4C and 4D show the extracted R_g and I_0 for all studied P188 concentrations. While the turbidity boundary depends slightly on the concentration of P188 (Fig. 2A), this unimer-micelle transition appears largely insensitive to P188 concentration. The unimer-micelle boundary is also shown by the green line in Fig. 2A.

Although R_g increases when the phenol concentration is above the unimer-micelle transition, its value plateaus when the concentration is sufficiently high (Fig. 4C), where formed micelles reach a certain size and cannot grow any larger. Changing the P188 concentration has no substantial impact on the size of the formed micelles. However, the total molecular mass of micelles is a function of P188 and phenol concentration, as indicated by the growth in I_0 with increasing phenol content (Fig. 4D). For a given P188 concentration, I_0 is proportional to the molecular mass of micelles in the solution. The continual increase in I_0 paired with the plateau in R_g as the concentration of phenol is increased indicates that micelles grow in molecular mass without growing larger in size. By normalizing I_0 to the concentration of P188, the results at different P188 concentrations can be compared directly. The normalized intensity is proportional to the product of two quantities: aggregation number of P188 and the mass of phenol relative to that of P188 in each micelle. The normalized intensity in the micelle region is smaller for higher concentrations of P188. Thus, increasing the concentration of P188 either

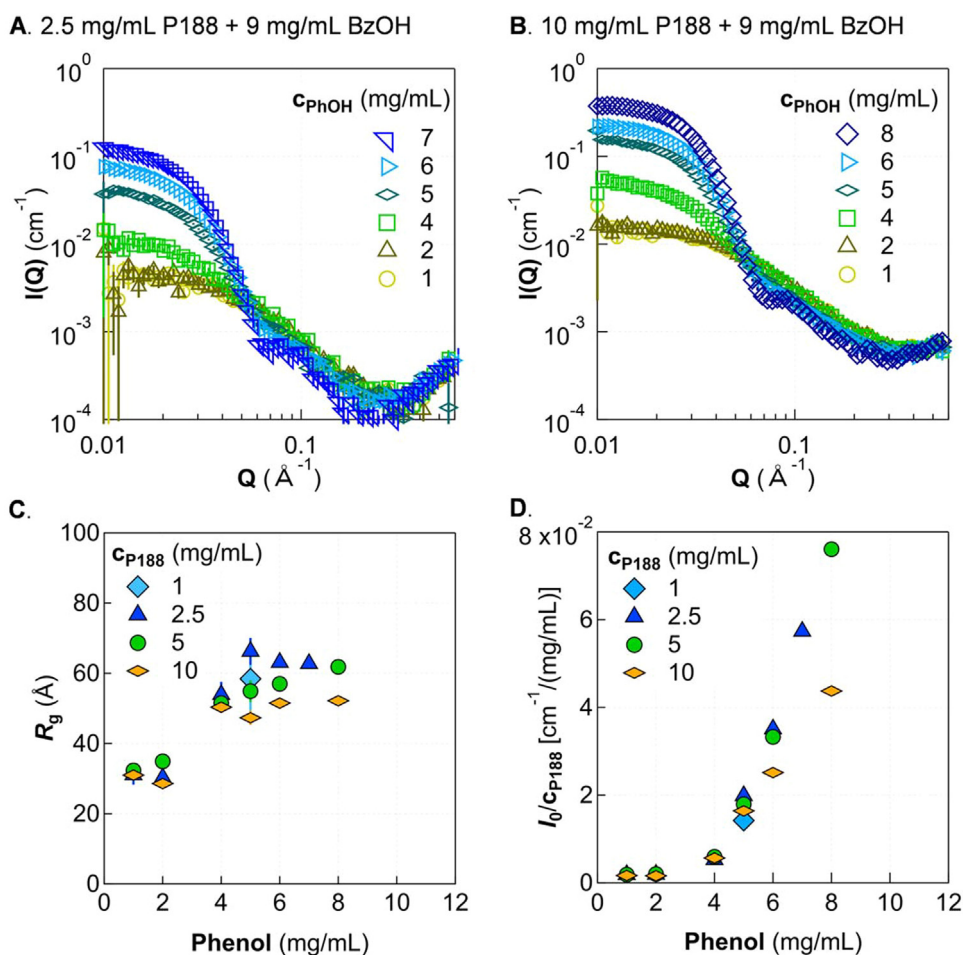


Fig. 5. Incorporation of 9 mg/mL benzyl alcohol causes increased scattering intensity at low- Q and a decreased unimer-micelle transition. SAXS patterns are shown for two representative concentrations of P188, 2.5 mg/mL (A) and 10 mg/mL (B), with benzyl alcohol fixed at 9 mg/mL and phenol concentration varied. Guinier analysis shows that R_g increases after a certain phenol concentration then tapers off as phenol is increased further (C), while I_0/c_{P188} (D) continues to increase as the turbidity boundary is approached. Solutions were in 5 mmol/L phosphate buffer at 20°C. Error bars are shown for all data and represent one standard deviation. Some error bars are covered by the markers.

decreases the total aggregation number of P188 in a micelle and/or decreases the amount of phenol in each micelle.

Based on the observed trends in R_g and I_0 with increasing c_{PhOH} , namely, that R_g initially increases to ~ 60 Å then stays around that size, while I_0 continues to linearly increase with c_{PhOH} , it is likely that phenol associates strongly with the hydrophobic core of individual P188 chains, then recruits additional P188 to form micelles. As more phenol is added, the hydrophobic core of the micelle swells with phenol. Increasing mass at the center would not appreciably affect R_g , but would indeed cause a continued rise in I_0 , which depends on molecular mass of aggregates. This is consistent with a previous NMR study where it was observed that the chemical shift of PPO methyl protons is affected first as phenol concentration is increased, indicating that phenol is interacting with the hydrophobic part of the polymer primarily before interacting with the PEO groups.¹⁷

From the trend in I_0 and R_g as the phenol concentration is increased toward the turbidity boundary, we speculate that precipitation of turbid compositions is related to the stability of the micelles as phenol concentration is increased. Based on SAXS data, adding more phenol in solution increases the amount of phenol in each micelle. When the amount of phenol in a micelle exceeds some threshold level, the micelle could become unstable. There are potentially two likely scenarios for the mechanism of precipitation that are still under investigation: (i) the micelles could become attractive to each other and form large aggregates, or (ii) the micelles could transition from a complex with finite size to another much larger-scale structure. However,

more investigation is needed to determine the exact mechanism for macroscopic phase separation in the turbid regime.

Effect of benzyl alcohol on the unimer-micelle transition

Multiple preservatives are sometimes utilized in a single drug product to achieve greater overall antimicrobial activity while remaining within the allowed dosage of individual ingredients. We therefore explored the effect of combining both phenol and benzyl alcohol with P188. SAXS for up to 10 mg/mL of benzyl alcohol in solution alone was indistinguishable from buffer (Fig. S1 in Supplementary Information). Hence, we see no evidence of aggregation of benzyl alcohol alone in the studied concentration region and Q -range.

R_g and I_0 for P188/phenol mixtures containing 9 mg/mL benzyl alcohol follow a similar trend with phenol concentration as solutions without benzyl alcohol (Fig. 5). Samples with phenol concentrations at or below 2 mg/mL generate scattering profiles indistinguishable from the P188-alone case; then low- Q scattering intensity increases for $c_{PhOH} \geq 4$ mg/mL, irrespective of P188 concentration (Fig. 5C). As was observed for the turbidity boundary, the unimer-micelle transition occurs at a lower phenol concentration of ≈ 4 mg/mL phenol when 9 mg/mL benzyl alcohol is present. As the phenol concentration approaches the threshold for turbidity, R_g (Fig. 5C) is observed to reach an apparent plateau value similar to that observed in mixtures without benzyl alcohol (Fig. 4C). Therefore, adding benzyl alcohol

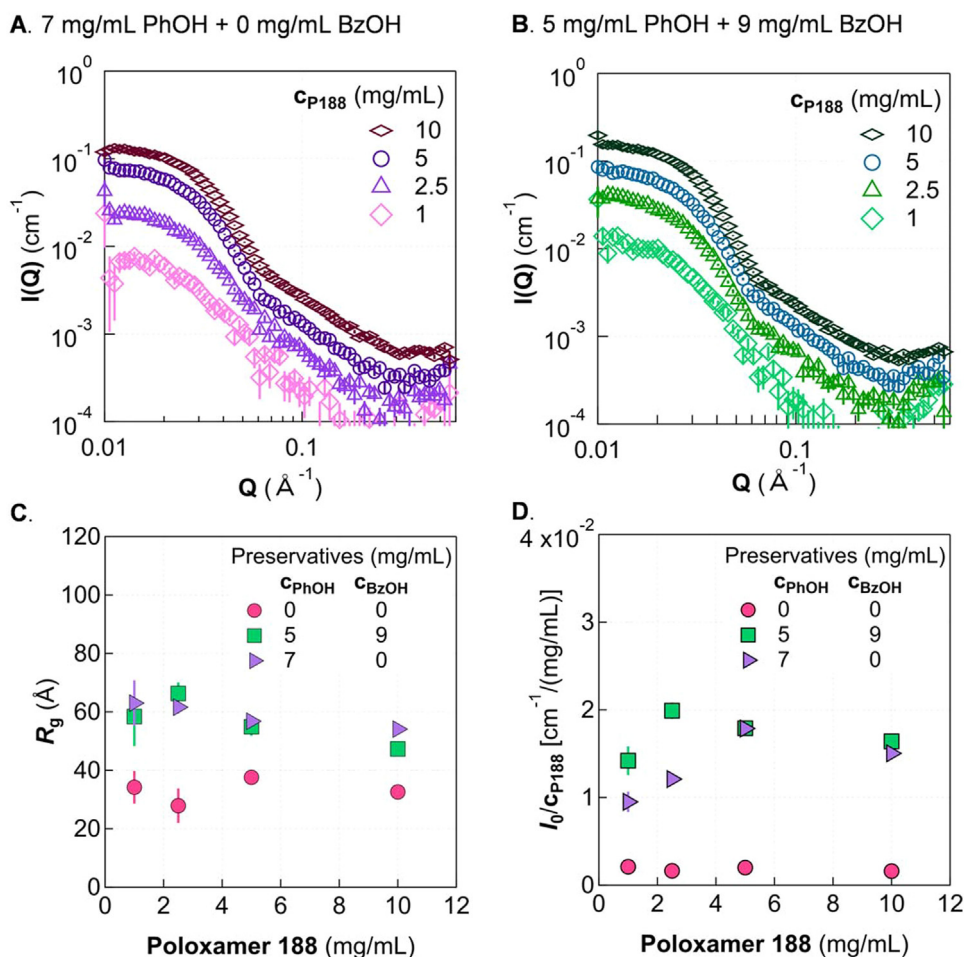


Fig. 6. Effect of P188 concentration in the micelle regime. A. In the absence of benzyl alcohol, 7 mg/mL phenol induces micelle formation with P188. B. With 9 mg/mL benzyl alcohol incorporated, 5 mg/mL phenol leads to micelle formation. Guinier analysis shows similar R_g (C) and I_0/C_{P188} (D) for the two preservative compositions. R_g and I_0/C_{P188} are shown for the no-preservative case for comparison. Solutions were in 5 mmol/L phosphate buffer at 20°C. Error bars are shown for all data and represent one standard deviation. Some error bars are covered by the markers.

does not seem to change the size of the formed micelles despite the shift of the transition concentration of phenol. The unimer-micelle phase boundary is shown by the green line in Fig. 2B as well.

The trend of the normalized I_0 (Fig. 5D) shows similar behavior as that in cases without benzyl alcohol (Fig. 4D). The molecular mass of individual micelles continues increasing with increasing phenol concentration, and the normalized intensity is smaller for higher concentrations of P188. When comparing the normalized intensity between Fig. 5D (with benzyl alcohol) and Fig. 4D (without benzyl alcohol) at similar concentrations of P188 and phenol, adding benzyl alcohol increases the total molecular mass of individual micelles. Therefore, even though adding benzyl alcohol does not appreciably affect the size of individual micelles, benzyl alcohol does increase the molecular mass of micelles and shifts the transition concentration between unimer and micelle. The consistent trends in R_g and I_0 with increasing C_{PhOH} suggests a similar mechanism of micelle formation when benzyl alcohol is added to P188/phenol solutions to that described above for the P188/phenol system.

We also visually evaluated P188/benzyl alcohol mixtures without phenol. Interestingly, we did not observe any turbidity through visual inspection even up to $C_{BzOH} = 18$ mg/mL. The reason that benzyl alcohol does not induce turbidity while phenol does at a given concentration of preservative remains unclear. This observation seems counterintuitive because benzyl alcohol is more hydrophobic than phenol. While the decreases in critical phenol

concentrations for micellization and turbidity upon the addition of benzyl alcohol are to be expected, the fact that phenol remains the determining factor in these phase transitions despite being less hydrophobic than benzyl alcohol was surprising. A possible explanation is that the alcohol moiety of benzyl alcohol is more flexible than in phenol, being on an sp^3 carbon instead of an aromatic sp^2 , so benzyl alcohol is less likely to pack tightly. Further investigation is needed to determine whether this is the cause for discrepancy between the effect of phenol and the effect of benzyl alcohol.

Morphology within the micelle regime

Having evaluated the effects of varied phenol concentration for fixed concentrations of P188 and benzyl alcohol, we sought to assess the effect of P188 concentration within the micelle regime with and without benzyl alcohol (Fig. 6). Holding phenol at approximately 1 mg/mL above the minimum phenol threshold required for micellization for each composition of benzyl alcohol, the scattering patterns are remarkably similar (Fig. 6A & B). This consistency suggests that micelles have similar morphology both with and without benzyl alcohol. Moreover, adding benzyl alcohol does not appreciably shift the size (Fig. 6C) or molecular mass (Fig. 6D) of micelles, despite there being more cumulative mass of preservatives in samples containing benzyl alcohol.

While the encapsulation of relatively hydrophobic molecules in a hydrophobic micelle core is commonly utilized in drug formulations, such as for liposomal drug delivery,³¹ the micellization observed here in P188/preservative mixtures is a combined effect due to the interplay between P188 and phenol. Several micellar systems, including other poloxamers, undergo a sphere-to-rod transition and subsequent micellar growth with the addition of phenol or phenolic derivatives^{32–34}; this phenol-induced transition has been explored for conditions already above the critical micelle concentration (CMC) or CMT of the respective surfactant. Our results, by contrast, show that phenol induces micelle formation of P188, not merely micellar growth or reorganization. Given that phenol concentration must exceed a certain threshold before micelles with P188 are formed, not all phenol is likely to be sequestered within micelles. We expect that free phenol remains active as an antimicrobial agent. However, the antimicrobial activity of phenol (and benzyl alcohol) that is associated with P188 micelles is less clear, as it depends on whether there is exchange between free and associated phenols. It should be pointed out that the influence of protein on P188/preservative micelle formation (and the efficacy of P188/preservative micelles in preventing protein aggregation) can be complicated as it is dictated by the interaction among protein, surfactant, and phenol. If there is no strong bonding between P188 and the protein—similar to the system reported recently by Zhang et al.³⁵—we would speculate that the formation of micelles would not be affected appreciably by the presence of protein. That said, if there is a strong interaction between P188 and protein, the issue is more complex and needs future study.

Conclusions

We have systematically studied micelle formation and turbidity in P188/phenol/phosphate buffer mixtures, both with and without benzyl alcohol, at room temperature (20°C to 22°C). Each individual component (P188, phenol, and benzyl alcohol) in buffer does not form micelles or aggregates within the studied concentration regions and Q-ranges. When P188 is combined with phenol, mixtures can become turbid at concentrations well below the phenol solubility limit. However, no turbidity or aggregation is observed when combining P188 and benzyl alcohol without phenol. Using SAXS, we found that there is a micelle regime below the turbidity boundary for both the P188/phenol system and the P188/phenol/benzyl alcohol system. The unimer-micelle transition occurs at a phenol concentration of around 6 mg/mL in the absence of benzyl alcohol and 4 mg/mL when 9 mg/mL benzyl alcohol is incorporated. These critical concentrations appear insensitive to P188 concentration, for the concentrations studied here ($c_{P188} \geq 2.5$ mg/mL). Below this micelle regime, P188 chains appear to be uniformly dispersed as unimers with a radius of gyration of about 30 Å. Above the critical phenol concentration, P188 and phenol (and benzyl alcohol) form micelles, whose radius of gyration increases initially then plateaus around 60 Å as the concentration of phenol is increased. The molecular mass of individual micelles continually increases as a function of phenol concentration before reaching the turbidity boundary, indicating that the ratio of phenol to P188 within micelles increases with increasing c_{PhOH} .

Structures in the micelle and unimer regimes appear stable; no visual change is observed for several weeks after mixing. This indicates that P188/preservative aggregation proceeds by a fundamentally different mechanism than the slow kinetics of PS80/preservative aggregation^{18,19} (in which initially transparent mixtures of PS80 and *m*-cresol at certain compositions become turbid over the course of several days). Mixtures of P188 and preservatives in the turbid regime undergo large scale phase separation after a few days, depositing precipitants or films on the walls of the vessel. The boundaries between unimer, micelle, and turbid regimes differs between solutions containing 9 mg/mL benzyl alcohol and those without: In

general, the phenol concentration for both the unimer-micelle transition and the turbidity boundary are about 2 mg/mL lower when 9 mg/mL of benzyl alcohol is included, as shown in Fig. 2. While benzyl alcohol does not alter the size of the micelles, it does increase the molecular mass of individual micelles. Our results provide valuable structural information relevant to pharmaceutical formulations containing P188 and small-molecule preservatives.

Declaration of interests

The authors declare that they have no known competing financial interests or personal relationships that could have appeared to influence the work reported in this paper.

Acknowledgements

Certain commercial equipment, instruments, or materials (or suppliers, or software, ...) are identified in this paper to foster understanding. Such identification does not imply recommendation or endorsement by the National Institute of Standards and Technology, nor does it imply that the materials or equipment identified are necessarily the best available for the purpose. This work is based upon research conducted at the Center for High Energy X-ray Sciences (CHEXS), which is supported by the National Science Foundation under award DMR-1829070, and the Macromolecular Diffraction at CHESS (MacCHESS) facility, which is supported by award 1-P30-GM124166-01A1 from the National Institute of General Medical Sciences, National Institutes of Health, and by New York State's Empire State Development Corporation (NYSTAR).

Supplementary materials

Supplementary material associated with this article can be found, in the online version, at doi:10.1016/j.xphs.2022.09.019.

References

- Paschen CA, Klemm D, Graf T, et al. Simultaneous quantification of polysorbate 20 and poloxamer 188 in biopharmaceutical formulations using evaporative light scattering detection. *J Pharm Biomed Anal.* 2021;192: 113640. <https://doi.org/10.1016/j.jpba.2020.113640>.
- Gualandi-Signorini AM, Giorgi G. Insulin formulations – a review. *Eur Rev Med Pharmacol Sci.* 2001;5:73–83.
- Bodratti A, Alexandridis P. Formulation of poloxamers for drug delivery. *JFB.* 2018;9(1):11. <https://doi.org/10.3390/jfb9010011>.
- Carpenter JF, Randolph TW, Jiskoot W, et al. Overlooking subvisible particles in therapeutic protein products: gaps that may compromise product quality. *J Pharm Sci.* 2009;98(4):1201–1205. <https://doi.org/10.1002/jps.21530>.
- Rosenberg AS. Effects of protein aggregates: an immunologic perspective. *AAPS J.* 2006;8(3):E501–E507. <https://doi.org/10.1208/aapsj080359>.
- Grapentin C, Müller C, Kishore RSK, et al. Protein-polydimethylsiloxane particles in liquid vial monoclonal antibody formulations containing poloxamer 188. *J Pharm Sci.* 2020;109(8):2393–2404. <https://doi.org/10.1016/j.xphs.2020.03.010>.
- Dwivedi M, Blech M, Presser I, Garidel P. Polysorbate degradation in biotherapeutic formulations: identification and discussion of current root causes. *Int J Pharm.* 2018;552(1–2):422–436. <https://doi.org/10.1016/j.ijpharm.2018.10.008>.
- Doshi N, Martin J, Tomlinson A. Improving prediction of free fatty acid particle formation in biopharmaceutical drug products: incorporating ester distribution during polysorbate 20 degradation. *Mol Pharmaceutics.* 2020;17(11):4354–4363. <https://doi.org/10.1021/acs.molpharmaceut.0c00794>.
- Moghimi SM, Hunter AC, Dadswell CM, Savay S, Alving CR, Szebeni J. Causative factors behind poloxamer 188 (Pluronic F68, FloCor™)-Induced complement activation in human sera. *Biochim Biophys Acta.* 2004;1689(2):103–113. <https://doi.org/10.1016/j.bbadis.2004.02.005>.
- Tsoneva I, Iordanov I, Berger AJ, et al. Electrodilution of Drugs into Cancer Cells in the Presence of Poloxamer 188. *J Biomed Biotechnol.* 2010;2010:1–11. <https://doi.org/10.1155/2010/314213>.
- Knoch H, Ulbrich MH, Mittag JJ, Buske J, Garidel P, Heerklotz H. Complex micellization behavior of the polysorbates Tween 20 and Tween 80. *Mol Pharmaceutics.* 2021;18(8):3147–3157. <https://doi.org/10.1021/acs.molpharmaceut.1c00406>.
- Tomlinson A, Zarraga IE, Demeule B. Characterization of polysorbate ester fractions and implications in protein drug product stability. *Mol Pharmaceutics.* 2020;17(7):2345–2353. <https://doi.org/10.1021/acs.molpharmaceut.0c00093>.

13. Singh SM, Bandi S, Jones DNM, Mallela KMG. Effect of polysorbate 20 and polysorbate 80 on the higher-order structure of a monoclonal antibody and its Fab and fragments probed using 2D nuclear magnetic resonance spectroscopy. *J Pharm Sci.* 2017;106(12):3486–3498. <https://doi.org/10.1016/j.xphs.2017.08.011>.
14. EMD Serono. Inc. *Gonal-F® RFF Redi-Ject® (Follitropin Alfa Injection) for Subcutaneous Use: Full Prescribing Information.* 2020.
15. Novo Nordisk. Inc. *Norditropin® (Somatropin) Injection, for Subcutaneous Use: Full Prescribing Information.* 2017.
16. Sandoz Inc. *Omnitrope (Somatropin) Injection: Full Prescribing Information.* 2019.
17. Jacobs J, Anderson RA, Watson TR. Nuclear magnetic resonance studies of interactions between oxyethylene-oxypropylene polymer, macroglol and phenol. *J Pharm Pharmacol.* 1972;24(7):586–589. <https://doi.org/10.1111/j.2042-7158.1972.tb09066.x>.
18. Gilbert PH, Zhang Z, Qian KK, Allen DP, Wagner NJ, Liu Y. Preservative induced polysorbate 80 micelle aggregation. *J Pharm Sci.* 2021;110(6):2395–2404. <https://doi.org/10.1016/j.xphs.2020.12.030>.
19. Gilbert PH, Zhang Z, Qian KK. Aggregation kinetics of polysorbate 80/m-cresol solutions: a small-angle neutron scattering study. *Mol Pharm.* 2022. <https://doi.org/10.1021/acs.molpharmaceut.1c00803>. [acs.molpharmaceut.1c00803](https://doi.org/10.1021/acs.molpharmaceut.1c00803).
20. Zhou Z, Chu B. Light-scattering study on the association behavior of triblock polymers of ethylene oxide and propylene oxide in aqueous solution. *J Colloid Interface Sci.* 1988;126(1):171–180. [https://doi.org/10.1016/0021-9797\(88\)90111-7](https://doi.org/10.1016/0021-9797(88)90111-7).
21. Hopkins JB, Gillilan RE, Skou S. *BioXTAS RAW: Improvements to a free open-source program for small-angle x-ray scattering data reduction and analysis.* *J Appl Crystallogr.* 2017;50(5):1545–1553. <https://doi.org/10.1107/S1600576717011438>.
22. Kline SR. Reduction and analysis of SANS and USANS data using IGOR Pro. *J Appl Crystallogr.* 2006;39(6):895–900. <https://doi.org/10.1107/S0021889806035059>.
23. Boualem Hammouda. 2022. Chapter 28: Form Factors for Polymer Systems. In *Probing Nanoscale Structures – The SANS Toolbox*; pp 288–300.
24. Doucet M, Cho JH, Alina G, et al. *SasView.* 2021.
25. National Center for Biotechnology Information. *PubChem Annotation Record for PHENOL. Hazardous Substances Data Bank (HSDB); 2022.*
26. Kim M, Vala M, Ertsgaard CT, et al. Surface plasmon resonance study of the binding of PEO–PPO–PEO Triblock Copolymer and PEO homopolymer to supported lipid bilayers. *Langmuir.* 2018;34(23):6703–6712. <https://doi.org/10.1021/acs.langmuir.8b00873>.
27. Wu YL, Sprik R, Poon W, Eiser E. Effect of salt on the phase behaviour of F68 Triblock PEO/PPO/PEO Copolymer. *J PHYS-CONDENS MAT.* 2006;18:4461–4470. <https://doi.org/10.1088/0953-8984/18/19/002>.
28. Chaghi R, de Ménorval L-C, Charnay C, Derrien G, Zajac J. Interactions of phenol with cationic micelles of hexadecyltrimethylammonium bromide studied by titration calorimetry, conductivity, and 1H NMR in the range of low additive and surfactant concentrations. *J Colloid Interface Sci.* 2008;326(1):227–234. <https://doi.org/10.1016/j.jcis.2008.07.035>.
29. Lippold H, Findeisen M, Quitzsch K, Helmstedt M. Micellar Incorporation without solubilizing effect. A study on the system water-phenol-decanoyl-n-methylglucamide. *Colloids Surf A.* 1998;135(1–3):235–244. [https://doi.org/10.1016/S0927-7757\(97\)00247-1](https://doi.org/10.1016/S0927-7757(97)00247-1).
30. Parekh P, Singh K, Marangoni DG, Aswal VK, Bahadur P. Solubilization and Location of Phenol and Benzene in a Nonlinear Amphiphilic EO–PO Block Copolymer Micelles: 1H NMR and SANS Studies. *Colloids Surf A.* 2012;400:1–9. <https://doi.org/10.1016/j.colsurfa.2012.02.029>.
31. Pattni BS, Chupin VV, Torchilin VP. New developments in liposomal drug delivery. *Chem Rev.* 2015;115(19):10938–10966. <https://doi.org/10.1021/acs.chemrev.5b00046>.
32. Mata JP, Aswal VK, Hassan PA, Bahadur P. A phenol-induced structural transition in aqueous cetyltrimethylammonium bromide solution. *J Colloid Interface Sci.* 2006;299(2):910–915. <https://doi.org/10.1016/j.jcis.2006.02.032>.
33. Dharaiya N, Bahadur P. Phenol Induced Growth in Triton X-100 Micelles: effect of PH and Phenols' hydrophobicity. *Colloids Surf A.* 2012;410:81–90. <https://doi.org/10.1016/j.colsurfa.2012.06.021>.
34. Mata JP, Majhi PR, Kubota O, Khanal A, Nakashima K, Bahadur P. Effect of phenol on the aggregation characteristics of an ethylene oxide–propylene oxide triblock copolymer P65 in aqueous solution. *J Colloid Interface Sci.* 2008;320(1):275–282. <https://doi.org/10.1016/j.jcis.2007.12.033>.
35. Zhang Z, Marie Woys A, Hong K, et al. Adsorption of non-ionic surfactant and monoclonal antibody on siliconized surface studied by neutron reflectometry. *J Colloid Interface Sci.* 2021;584:429–438. <https://doi.org/10.1016/j.jcis.2020.09.110>.